

Role of Promoters on the Acrolein Ammoxidation Performances of BiMoO_x

Ajay Ghalwadkar¹ · Benjamin Katryniok¹ · Sébastien Paul¹ · Anne-Sophie Mamede¹ · Franck Dumeignil^{1,2,3}

Received: 1 September 2015 / Revised: 21 December 2015 / Accepted: 21 December 2015 / Published online: 12 January 2016
© AOCS 2016

Abstract Ammoxidation of acrolein to acrylonitrile was studied using multicomponent (MC) BiMoO_x catalysts in the presence of ammonia and oxygen. The MC catalysts containing bivalent and trivalent metal promoters were found to be highly active and selective to acrylonitrile. The corresponding MC catalysts were characterized by X-ray diffraction, nitrogen physisorption, X-ray photoelectron spectroscopy, ICP-MS and UV–visible diffuse reflectance spectroscopy. It was observed that, among the bivalent cations, the catalysts containing both Co–Ni showed superior performances due to the presence of the metastable β -Co_xNi_{1-x}MoO₄ phase. The presence of a trivalent cation, and especially of iron, promoted the formation of both the γ -Bi₂MoO₆ active phase and the active β -phase of bivalent metal molybdate. Further, optimization of the reaction conditions enabled the achievement of a 59 % acrylonitrile yield.

Keywords Glycerol · Ammoxidation · Multicomponent catalysts · Acrolein · Acrylonitrile

Introduction

The depletion of fossil fuel resources combined with the rapidly growing worldwide vehicle fleets, from approximately 1 billion vehicles today to 1.6 billion vehicles forecast for 2030, notably brought the attention towards the exploration of renewable resources for the production of fuels such as, for instance, biodiesel, which can be obtained by transesterification of vegetable oils. The European Union has set the target of blending domestic petro-based fuels with 7 % of fuels derived from renewable resources by 2020 [1]. As a result, the biodiesel production has drastically increased, and it is predicted that it would reach about 42 million metric tons in 2020 [2]. Consequently, the amount of available glycerol, the main by-product of the biodiesel production process has also increased over the last decade and glycerol has thus become an attractive starting material for industrial processes [3]. One of the most promising ways for valorizing glycerol consists of its dehydration to acrolein (AC). The latter is an important building block for the syntheses of polyacrylate polymers and methionine [4, 5].

On the other hand, acrylonitrile (ACN) is placed among the top 50 chemicals produced in the US and is mainly utilized in the synthesis of acrylic fibers, Acrylonitrile–Butadiene–Styrene (ABS), Styrene–Acrylonitrile (SAN) resins, adiponitrile and acrylamide [6]. Currently, the dominant process for acrylonitrile production is the SOHIO process, which is based on propylene ammoxidation in the presence of air and ammonia over a multicomponent bismuth–molybdenum oxide catalyst [6]. Propane ammoxidation is an alternative process to propylene ammoxidation, with however a lower yield (60 vs 70 %) [7]. Recently, the ACN production by glycerol ammoxidation was reported using either direct or indirect ammoxidation of glycerol [4, 8].

Benjamin Katryniok and Franck Dumeignil: paper based on work presented at the AOCS Annual Meeting.

✉ Franck Dumeignil
franck.dumeignil@univ-lille1.fr

¹ CNRS, Centrale Lille, ENSCL, Univ. Artois, UMR 8181 - UCCS - Unité de Catalyse et Chimie du Solide, Univ. Lille, 59000 Lille, France

² IUF, Maison des Universités, 103 boulevard Saint-Michel, 75005 Paris, France

³ Unité de Catalyse et Chimie du Solide (UCCS), Université Lille 1, Sciences et Technologies, Bâtiment C3, 59655 Villeneuve d'Ascq Cedex, France

Guerrero-Perez *et al.* reported the direct conversion of glycerol to ACN in the presence of ammonia and oxygen over mixed oxides containing V, Sb and Nb. The highest ACN yield of 48 % is the subject of some debate [9, 10]. With respect to the possibility of choosing the catalyst and reaction conditions independently, Liebig *et al.* studied the two step conversion of glycerol to ACN with AC as an intermediate. They obtained an overall yield in ACN of 40 % at full glycerol conversion in an integrated tandem reactor process [5]. Whereas, the first step (the dehydration of glycerol to AC) has been widely studied [3], very little attention has been paid so far to the AC ammoxidation reaction.

A few AC ammoxidation catalysts are known in the literature. However, considering a tandem reaction with glycerol dehydration as the first step, the catalyst of the second step should be—at least—water-tolerant. The As–Fe–O, Fe₂O₃–Bi₂O₃–P₂O₅, and Fe–Sb–O mixed oxides were tested for AC ammoxidation in the presence of water. The As–Fe–O mixed oxide catalyst gave the highest ACN yield of 87.1 % at 400 °C [11]. However, the use of arsenic should be definitely avoided in an industrial process due to obvious toxicity issues.

Studying the ammoxidation reaction, Oka *et al.* [12] found an AC conversion rate 1000 times higher than that of propylene at 400 °C over a Fe₂O₃–Bi₂O₃–P₂O₅ catalyst in the presence of 51 % water (exhibiting a 40 % yield of ACN from AC). Liebig *et al.* reported a Fe–Sb–O catalyst for the AC ammoxidation reaction. The highest yield of 36 % in ACN was reported at 400 °C with around 86.8 % water in the feed [5].

With respect to the relatively low yields (<40 %) obtained in the ammoxidation of AC in the presence of water over specifically designed catalysts, we decided to focus our study on the multicomponent (MC) BiMoO_x-type catalysts. This kind of catalyst is well-known for its high performances in the oxidation and ammoxidation of olefins [13–15]. Bismuth phosphomolybdate was the first multicomponent catalyst of this family commercialized by SOHIO for propylene ammoxidation, with an ACN yield of 65 % at full conversion. Since the initial commercialization, several generations of improved catalysts with enhanced yields were developed by addition of promoters such as trivalent transition metals (especially Fe) [16], bivalent transition metals (i.e., Co and Ni) [17] and alkalis (notably K) [18].

Despite their high activity and selectivity in oxidation/ammoxidation reactions, it is still not clear how multicomponent bismuth molybdate catalysts show such high performances, due to their complex compositions and structures. It is known that these multicomponent catalysts comprise three major parts: the first one is bismuth molybdate, the second one is the trivalent metal molybdate (Fe³⁺) and the third one is a mixture or a solid solution of divalent metal molybdates (of Co²⁺, Ni²⁺ or Mg²⁺) [14, 15]. Bismuth molybdate exists

in three crystallographic forms: α-Bi₂Mo₃O₁₂, β-Bi₂Mo₂O₉ and γ-Bi₂MoO₆. However, there is no agreement on which phase is active and selective for the ammoxidation reaction. Kolchin *et al.* [19] and German *et al.* [20] stated that the activity follows the β > α > γ sequence for propene oxidation and ammoxidation, while Monnier and Keulks [21] claimed the order is γ > β > α (for propene oxidation), whereas Burrington and Grasselli [22] found that this order is β = α > γ for selective oxidation of propene. Furthermore, Carson *et al.* [23] suggested that there is a synergy effect between the α and the γ phases leading to better activity and selectivity for an intimate equimolar mixture.

Among the several compositions of multicomponent Bi–Mo–O_x catalysts tested for propylene ammoxidation to acrylonitrile, Co_{4.5}Ni_{2.5}Fe₃BiK_{0.07}P_{0.5}Mo₁₂O₅₅ with silica (17.5 wt%) as a binder is reported to show a high activity for acrylonitrile production with 80 % yield [18]. Therefore, we focused in the present study on the ammoxidation of AC to ACN over a multicomponent bismuth molybdate catalyst with the above composition. This MC catalyst contains mainly two kinds of promoters, namely (1) bivalent metals, i.e., Co and Ni and (2) a trivalent metal, i.e., Fe. Therefore, to study the effects of bivalent and trivalent metal cations, a series of multicomponent (MC) catalysts was synthesized and screened for the AC ammoxidation reaction to ACN. Furthermore, the reaction parameter optimization was performed using the design of experiments methodology.

Experimental Section

Catalyst Synthesis

The multicomponent Bi–Mo catalyst has as a general formula M^{II}M^{III}BiMo₁₂O_x where M^{II} is a bivalent metal and M^{III} is a trivalent metal. Therefore, the catalysts were synthesized according to two groups: group (1) with different M^{II} cations such as Co, Ni and Mg and group (2) with different M^{III} cations such as Fe, Cr and Al.

These multicomponent catalysts were prepared according to the co-precipitation method described in SOHIO patent [18] and their theoretical compositions are summarized in Table 1.

A typical synthesis procedure was as follows: Bi(NO₃)₃·5H₂O (Sigma Aldrich) was dissolved in a 5 M nitric acid solution at room temperature. When all the bismuth nitrate was dissolved, the appropriate amounts of Ni(NO₃)₂·6H₂O (Fluka), Co(NO₃)₂·6H₂O (Sigma Aldrich), and Fe(NO₃)₂·9H₂O (Acros Organics) were added to the solution. In a second flask, the appropriate amount of (NH₄)₆Mo₇O₂₇·4H₂O (Sigma Aldrich) was dissolved in 80 mL of water with minimum heating at 50 °C before the appropriate amount of KNO₃ (Sigma Aldrich) and H₃PO₄

Table 1 Theoretical composition of the series of MC catalysts

Catalyst	Composition	Silica (Binder) wt %
MC-A (reference)	Co _{4.5} Ni _{2.5} Fe ₃ BiK _{0.07} P _{0.5} Mo ₁₂ O ₅₅	17.5
MC-B (no Fe, K, P)	Co _{4.5} Ni _{2.5} BiMo ₈ O ₃₃	17.5
MC-C (no Ni)	Co ₇ Fe ₃ Bi K _{0.07} P _{0.5} Mo ₁₂ O ₅₅	17.5
MC-D (no Co)	Ni ₇ Fe ₃ Bi K _{0.07} P _{0.5} Mo ₁₂ O ₅₅	17.5
MC-E (no Bi, K, P)	Co _{4.5} Ni _{2.5} Fe ₃ Mo ₁₀ O ₄₂	17.5
MC-F (Mg replaces Co & Ni)	Mg ₇ Fe ₃ BiK _{0.07} P _{0.5} Mo ₁₂ O ₅₅	17.5
MC-G (Cr replaces Fe)	Co _{4.5} Ni _{2.5} Cr ₃ BiK _{0.07} P _{0.5} Mo ₁₂ O ₅₅	17.5
MC-H (Al replaces Fe)	Co _{4.5} Ni _{2.5} Al ₃ BiK _{0.07} P _{0.5} Mo ₁₂ O ₅₅	17.5

(85 %, Sigma Aldrich) were added to obtain a clear solution. Then, the initially prepared solution containing the nitrate precursors was added dropwise under continuous stirring to the second solution, whereby a precipitate was formed. Finally, colloidal silica (Ludox AM-30, Aldrich) was added to the precipitate as a binder before the solvent was evaporated at 80 °C. After drying at 150 °C for 24 h, the catalyst was calcined at 540 °C for 24 h under static air.

Catalyst Characterizations

The specific surface areas and pore volumes of the catalysts were measured by nitrogen adsorption at liquid nitrogen temperature (−196 °C) using a Micrometrics ASAP 2010 instrument. The specific surface area (SSA) was evaluated by using the multi-point BET method. The total pore volume (V_p) was calculated using the isotherms at the relative pressure (P/P_0) of 0.98.

The bulk composition of the catalysts was determined by Inductively Coupled Plasma spectroscopy on an Agilent Technologies 720 series instrument coupled with an optical emission spectra detector. Prior to analysis, all the catalysts were first dissolved in aqua regia and then a very small amount of HF was added in order to dissolve silica. Further dilution was performed by addition of deionized water.

Powder X-ray diffractograms were recorded on a Bruker D8 advance diffractometer, using the CuK α radiation ($\lambda = 1.5506 \text{ \AA}$) as an X-ray source, in the 2θ range of 10°–80° with integration steps of 0.02° (2θ) per second.

X-ray photoelectron spectroscopy (XPS) for surface analyses was carried out using a Kratos Axis Ultra DLD apparatus equipped with a hemispherical analyzer and a delay line detector. The spectra were recorded using an Al mono-chromated X-ray source (10 kV, 15 mA) with a pass energy of 40 eV (0.1 eV/step) for high resolution spectra, and a pass energy of 160 eV (1 eV/step) for survey spectrum in hybrid mode and slot lens mode, respectively. The adventitious C 1 s (285.0 eV) binding energy (BE) was used as an internal reference.

UV/Vis DRS analysis of solid catalysts was performed on a Perkin Elmer-Lambda 650S spectrometer.

Experimental Setup for Acrolein Ammoxidation Reaction

The catalytic performance was determined using 3.5 g catalyst at atmospheric pressure in a downflow fixed-bed reactor (20 cm length, 1.5 cm ID) at 390 °C. The aqueous solution of acrolein was introduced by means of an HPLC pump and evaporated before being mixed with the second reactant flow (namely oxygen or air), which was controlled by a mass-flow controller. The ammonia was added just before the gas mixture enters the catalyst bed to avoid any undesired polymerization of AC. The molar ratio of NH₃/AC and O₂/AC were set at 1.75 and 2.7, respectively. The reaction products were collected in a cold trap containing a 5 % aqueous acetic acid solution (in order to neutralize unreacted ammonia) at −5 °C and analysed by means of gas chromatography (Alltech EC-1000 semi-capillary column; 30 m; diameter: 0.53 mm; film thickness: 1.2 μm).

If not detailed otherwise, the main by-products in the acrolein ammoxidation reaction were CO and CO₂. The other by-products formed are acetaldehyde (selectivity usually around 2 %), acetonitrile (selectivity usually of around 2 %) and propionitrile (selectivity usually around 1 %). The typical carbon balance of the reaction is in the range of 88–94 %.

The optimization of reaction conditions was performed using a computer assisted experimental design generated by the statistical soft-ware Design-Expert, Version 5.0.8, Stat-Ease Inc. The response surface methodology was used in order to investigate the influence of the varied parameters (reaction temperature, contact time, molar NH₃/AC ratio) on the responses.

Results and Discussion

Acrolein Ammoxidation Reaction

The catalysts were screened according to two groups: group (a) with different M^{II} cations such as Co, Ni and Mg, and group (b) with different M^{III} cations such as Fe, Cr and Al.

Effect of Bivalent Metal Cations

Figure 1 shows the catalytic performances of group a) catalysts. The catalyst containing a combination of Co and Ni (MC-A) shows a higher acrolein conversion (87 %) than those of the catalysts containing one of these metals alone (81 % for MC-C–Co and 75 % for MC-D–Ni). The selectivity to acrylonitrile is rather the same (54 %) for the catalysts containing Co–Ni (MC-A) or only Co (MC-C). However, the Ni-containing catalyst (MC-D) exhibits a comparatively lower selectivity to acrylonitrile (48 %) and promotes the formation of total oxidation products (41 % selectivity to CO/CO₂). In other words, Co and Ni when used together (MC-A), give better performances in terms of acrylonitrile yield than when used alone. The by-products comprise acetonitrile, propionitrile and acetaldehyde.

Effect of Trivalent Metal Substitution

The influence of trivalent metal substitution was studied by removing or replacing Fe from the MC-A catalyst with Cr or Al. The results are shown in Fig. 2. The iron-free Co–Ni–Bi catalyst (MC-B) showed a relatively low acrolein

conversion (80 %) as well as a very low acrylonitrile selectivity (28 %) compared to the iron-containing MC-A catalyst (87 % conversion and 54 % selectivity). The catalyst activity significantly dropped when iron was replaced by Cr and Al, whereby Cr (MC-G) showed the lowest performances with 68 % acrolein conversion and 31 % selectivity to acrylonitrile. The Al-containing catalyst (MC-H) exhibited 80 % conversion and 39 % selectivity.

Catalysts Characterization

Textural Properties

The specific surface areas, pore volumes and mean pore diameters of the catalyst determined by nitrogen physisorption, are gathered in Table 2.

All the multicomponent catalysts exhibited specific surface areas in the range of 10–21 m²/g and a mean pore diameter in the range of 14–24 nm. The analysis of the spent catalysts shows that the specific surface area and pore volume had slightly decreased after the reaction, while the mean pore diameter had increased from 16–17 to 20–21 nm. The latter can be explained by the fact that the MC-catalysts are

Fig. 1 Effect of bivalent metal substitution on the catalytic performance [group (a) catalysts]. Reaction conditions: Temperature—390 °C, pressure—1 bar, catalyst wt.—3.5 g, contact time—0.5 s, NH₃/AC ratio—1.75, O₂/AC ratio—2.7, feed molar composition—Acr:NH₃:O₂:N₂:H₂O = 1.7:3:4.6:37:53

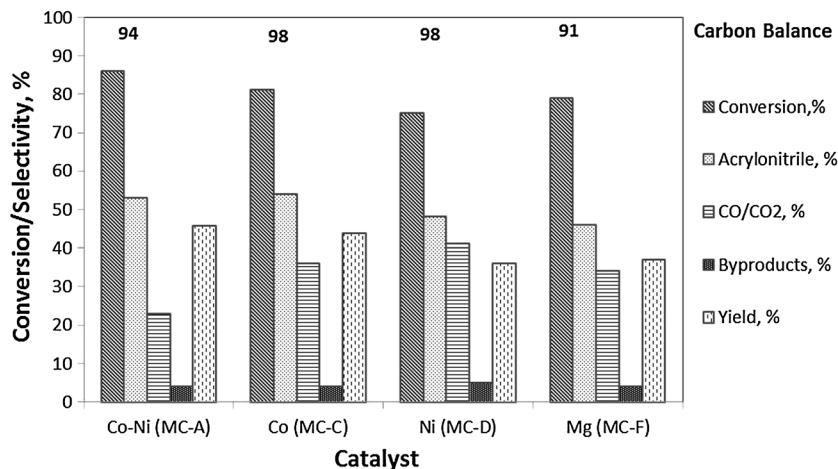


Fig. 2 Effect of trivalent cations [group (b) catalysts]. Reaction conditions: temperature—390 °C, pressure—1 bar, catalyst wt.—3.5 g, contact time—0.5 s, NH₃/AC ratio—1.75, O₂/AC ratio—2.7, feed molar composition—Acr:NH₃:O₂:N₂:H₂O = 1.7:3:4.6:37:53

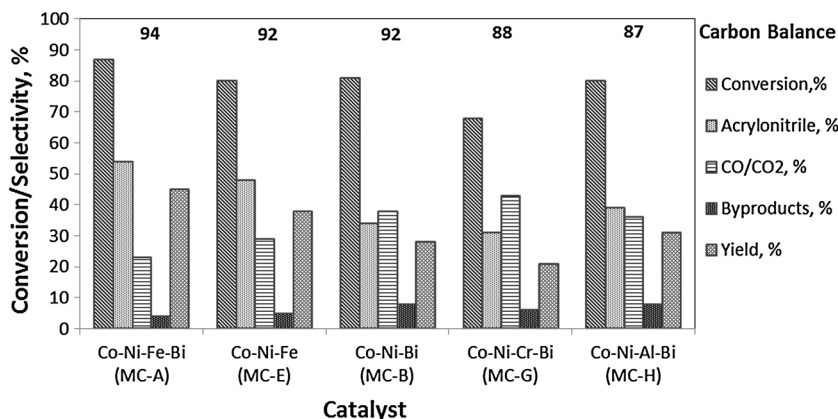


Table 2 Textural properties of the catalysts

Catalyst reference	SSA (m ² /g)	Mean pore diameter (nm)	Pore volume (cm ³ /g)
MC-A	15	16	0.077
MC-A (spent)	13	20	0.075
MC-B	19	17	0.091
MC-B (spent)	15	21	0.081
MC-C	18	18	0.08
MC-D	20	19	0.10
MC-E	21	16	0.10
MC-F	13	21	0.07
MC-G	10	24	0.065
MC-H	19	15	0.041

non-porous materials with broad pore size distribution. During the reaction, the amount of micropores decreases either by coke formation or by sintering. This loss of microporosity explains (1) the decrease in specific surface area of the spent catalyst and (2) the increase in the mean pore diameter.

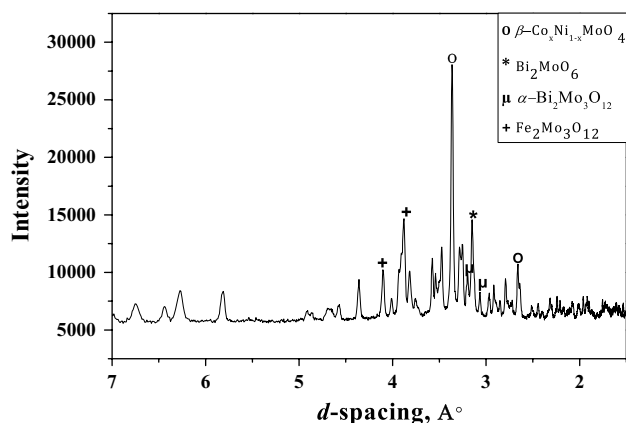
Bulk Composition of the Catalysts

The elemental compositions of the catalysts were determined by ICP-OES analysis (Table 3). The figures in Table 3 indicate that the theoretical and experimental compositions are close in all the cases. Nevertheless, there are some exceptions such as in the Ni content in MC-D and the Cr and Mo values in MC-G, which are lower than the theoretical ones. However, the results globally indicate that catalysts were successfully prepared by the coprecipitation method.

Phase Compositions by XRD

The diffractogram of multicomponent catalyst MC-A is exemplarily shown in Fig. 3. This catalyst exhibited a

complex diffraction pattern, which was of the same kind for all the MC catalysts. They thus consist of α and β forms of cobalt/nickel molybdates, trivalent iron molybdate ($\text{Fe}_2\text{Mo}_3\text{O}_{12}$) and α and γ forms of bismuth molybdate. Table 4 summarizes the phase compositions of the all multicomponent catalysts determined by X-ray diffraction. It can be seen that catalyst MC-A shows the formation of $\beta\text{-Co}_x\text{Ni}_{1-x}\text{MoO}_4$ with d values of 2.24, 2.31, 2.44, 2.79 and 3.36 Å [24]. The structure of this mixed compound is a solid solution of $\beta\text{-CoMoO}_4$ and $\beta\text{-NiMoO}_4$ in common molybdate lattice. In the case of the MC-B and MC-E catalysts, prepared without Fe and Bi, respectively, the formation of $\alpha\text{-Co}_x\text{Ni}_{1-x}\text{MoO}_4$ along with its β form is observed, the former being a solid solution of $\alpha\text{-CoMoO}_4$ and $\alpha\text{-NiMoO}_4$. The main difference between the α and β forms of Co/NiMoO_4 is the oxygen coordination of Mo which is tetrahedral in $\beta\text{-Co/NiMoO}_4$ and essentially octahedral in $\alpha\text{-Co/NiMoO}_4$. $\beta\text{-CoMoO}_4$ is stable at high temperature (above 678 K) and exists in a metastable state at room temperature, whereas $\alpha\text{-CoMoO}_4$ is stable at low temperature (below 678 K) [25]. The MC-G and MC-H catalysts also

**Fig. 3** XRD diffractogram of MC-A**Table 3** Elemental composition of the catalysts (determined by ICP-OES) normalized to 1 mol of Bi

Catalyst	Co		Ni		Fe		Bi		Mo		P		K	
	Th	Ex	Th	Ex	Th	Ex	Th	Ex	Th	Ex	Th	Ex	Th	Ex
MC-A	4.5	4.8	2.5	2.4	3	3	1	1	12	11.4	0.5	0.6	0.07	0.09
MC-B	4.5	4.3	2.5	2.3	–	–	1	1	8	10.9	–	–	–	–
MC-C	7	6.7	–	–	3	2.8	1	1	12	10.9	0.5	0.6	0.07	0.05
MC-D	–	–	7	5.6	3	2.7	1	1	12	10.4	0.5	0.6	0.07	0.05
MC-E	4.5	4.5	2.5	2.7	3	3	–	–	10	12	–	–	–	–
MC-F	–	–	7 ^a	6.3	3	2.7	1	1	12	10.7	0.5	0.5	0.07	0.06
MC-G	4.5	4	2.5	2.1	3 ^b	1.5	1	1	12	9	0.5	0.5	0.07	0.08
MC-H	4.5	4.2	2.5	2.3	3 ^c	2.8	1	1	12	10.5	0.5	0.5	0.07	0.05

Th theoretical, Ex experimental

^a Mg, ^bCr and ^cAl

Table 4 Phase composition of the multicomponent catalysts

Catalyst	Composition/wt% silica	Phases obtained	<i>d</i> -spacing ^a (Å)	Relative intensity, I ^b	Ratio ^c
MC-A	Co _{4.5} Ni _{2.5} Fe ₃ BiK _{0.07} P _{0.5} Mo ₁₂ O ₅₅ /17.5	β -Co _x Ni _{1-x} MoO ₄	3.36	100	2.6
		Fe ₂ Mo ₃ O ₁₂	3.88	38.6	
		γ -Bi ₂ MoO ₆	3.15	39.1	
		α -Bi ₂ Mo ₃ O ₁₂	3.19	15.8	
MC-B	Co _{4.5} Ni _{2.5} BiMo ₈ O ₃₃ /17.5	α -Co _x Ni _{1-x} MoO ₄	3.13	68.7	0.6
		β -Co _x Ni _{1-x} MoO ₄	3.37	100	
		γ -Bi ₂ MoO ₆	3.15	43.7	
		α -Bi ₂ Mo ₃ O ₁₂	3.19	71.2	
		MoO ₃	3.82	55	
MC-C	Co ₇ Fe ₃ BiK _{0.07} P _{0.5} Mo ₁₂ O ₅₅ /17.5	β -CoMoO ₄	3.37	100	4.37
		Fe ₂ Mo ₃ O ₁₂	3.88	26.3	
		γ -Bi ₂ MoO ₆	3.15	36.3	
		α -Bi ₂ Mo ₃ O ₁₂	3.19	8.3	
MC-D	Ni ₇ Fe ₃ BiK _{0.07} P _{0.5} Mo ₁₂ O ₅₅ /17.5	α -NiMoO ₄	3.34	100	4.37
		Fe ₂ Mo ₃ O ₁₂	3.88	43.8	
		γ -Bi ₂ MoO ₆	3.15	37.7	
		α -Bi ₂ Mo ₃ O ₁₂	3.20	8.9	
MC-E	Co _{4.5} Ni _{2.5} Fe ₃ Mo ₁₂ O ₄₂ /17.5	α -Co _x Ni _{1-x} MoO ₄	3.12	47.9	–
		β -Co _x Ni _{1-x} MoO ₄	3.36	100	
		Fe ₂ Mo ₃ O ₁₂	3.87	41.8	
		α -NiMoO ₄	6.25	41.3	
MC-F	Mg ₇ Fe ₃ BiK _{0.07} P _{0.5} Mo ₁₂ O ₅₅ /17.5	β -MgMoO ₄	3.38	100	1.74
		Fe ₂ Mo ₃ O ₁₂	3.88	51.5	
		γ -Bi ₂ MoO ₆	3.15	57.8	
		α -Bi ₂ Mo ₃ O ₁₂	3.19	33.1	
MC-G	Co _{4.5} Ni _{2.5} Cr ₃ BiK _{0.07} P _{0.5} Mo ₁₂ O ₅₅ /17.5	α -Co _x Ni _{1-x} MoO ₄	3.12	11.6	1.27
		β -Co _x Ni _{1-x} MoO ₄	3.36	100	
		Cr ₂ Mo ₃ O ₁₂	3.85	27.8	
		γ -Bi ₂ MoO ₆	3.15	13.9	
		α -Bi ₂ Mo ₃ O ₁₂	3.18	10.9	
MC-H	Co _{4.5} Ni _{2.5} Al ₃ BiK _{0.07} P _{0.5} Mo ₁₂ O ₅₅ /17.5	α -Co _x Ni _{1-x} MoO ₄	3.13	17.9	0.71
		β -Co _x Ni _{1-x} MoO ₄	3.36	100	
		Al ₂ Mo ₃ O ₁₂	3.81	32.9	
		γ -Bi ₂ MoO ₆	3.15	29.3	
		α -Bi ₂ Mo ₃ O ₁₂	3.19	41.3	

^a *d*-spacing is the interplanar spacing of the most intense main line of the corresponding phase

^b Relative Intensity I is the intensity of the main line of the corresponding phase, as a percentage of the line intensity of β -CoMoO₄

^c Ratio of relative intensities of γ -Bi₂MoO₆ and α -Bi₂Mo₃O₁₂ peaks

contain the α -Co_xNi_{1-x}MoO₄ phase, but with peaks exhibiting a lower relative intensity. In the MC-C catalyst (without Ni) the formation of the metastable β -CoMoO₄ phase is clearly identified through the most intense peak at 3.37 Å (JC-PDS 21-0868). On the other hand, the catalyst MC-D (in absence of Co) exhibits the formation of α -NiMoO₄ as evidenced from *d* values of 3.10 and 3.34 Å (JC-PDS 33-0948) [26]. In fact, it is reported that β -NiMoO₄ cannot be quenched at ambient temperature unlike the isotypic

CoMoO₄, and undergoes phase transformation from β to α when decreasing temperature [27].

In all the catalysts, bismuth was present in two forms: γ -Bi₂MoO₆, and α -Bi₂Mo₃O₁₂. The peaks observed at *d*-spacing values of 3.19 and 3.06 Å were assigned to α -Bi₂Mo₃O₁₂ (JC-PDS 21-0103), while the γ -Bi₂MoO₆ phase was identified from the peak at 3.15 Å (JC-PDS 21-0102). Nevertheless, the relative intensities of the peaks of the two phases are varying according to the

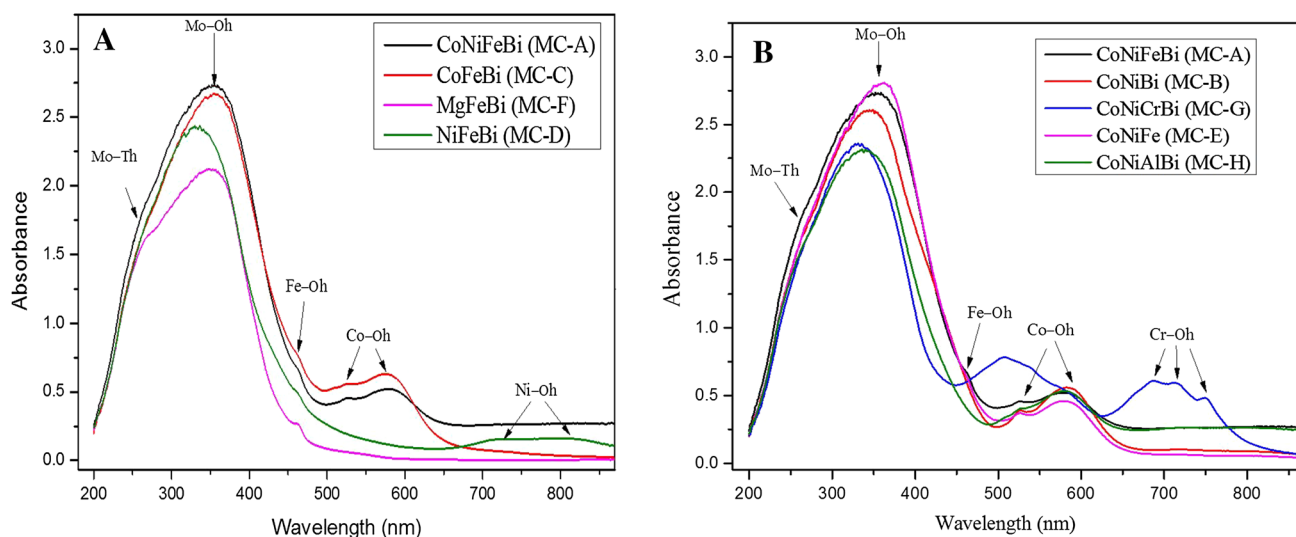


Fig. 4 UV/Vis diffuse reflectance spectra of multicomponent catalysts

catalysts. In the MC-B catalyst (in the absence of iron), the α - $\text{Bi}_2\text{Mo}_3\text{O}_{12}$ phase appears to be relatively better defined than the γ - Bi_2MoO_6 , whereas this is the reverse in the case of the MC-A catalyst—containing Fe—, which indicates that the presence of iron tends to promote the formation of the γ - Bi_2MoO_6 phase [28]. A similar trend is observed when Fe is substituted with Cr and Al (MC-G and MC-H). In the Cr-containing catalyst, the bismuth molybdate phases occur with peaks of a similar but lower intensities than in the MC-A catalyst, whereas the α -phase dominates over γ - Bi_2MoO_6 in Al-containing catalyst. Concerning iron, the latter is present in the trivalent iron molybdate form ($\text{Fe}_2\text{Mo}_3\text{O}_{12}$) in all the Fe-containing catalysts, which is obvious from the d value at 3.88 \AA (JC-PDS 31-0642). Similarly, Cr- and Al-containing catalysts form $\text{Cr}_2\text{Mo}_3\text{O}_{12}$ and $\text{Al}_2\text{Mo}_3\text{O}_{12}$ structures, respectively, which are isomorphous of $\text{Fe}_2\text{Mo}_3\text{O}_{12}$ [29, 30].

UV/Visible Diffuse Reflectance Spectroscopy

In order to obtain more information on the coordination of the metal ions, UV–Vis DRS spectra were recorded (Fig. 4). The spectra of the molybdate species exhibit charge-transfer transitions between O^{2-} and Mo^{6+} in the range starting from 480 nm [31]. All the multicomponent catalysts showed unusually broad peaks at around 245 nm and 360 nm, which were assigned to tetrahedral and octahedral molybdenum species, respectively [32, 33]. The β - CoMoO_4 and β - MgMoO_4 phases observed by XRD are in agreement with Mo in tetrahedral coordination, whereas octahedral Mo can belong to the γ - Bi_2MoO_6 , α - CoMoO_4 and α - NiMoO_4 phases [32].

The MC-C catalyst (Fig. 4a) showed two bands at 525 and 580 nm, indicating that Co is octahedrally coordinated by oxygen, suggesting the presence of the β - CoMoO_4 structure also found by XRD [34]. All the catalysts containing cobalt showed absorption in this region. The MC-D catalyst exhibited two bands at around 710 and 780 nm, suggesting that the Ni^{2+} is in octahedral coordination of oxygen [35]. However, for the Cr-containing catalyst (MC-G), these bands are covered by the stronger absorption of chromium molybdate (Fig. 4b). The magnesium-containing catalyst (MC-F) showed characteristics band of tetrahedral molybdenum. However, there is no specific band information observed for the coordination of Mg [36].

The iron-containing catalysts always exhibited a maximum at 460 nm, which is a characteristic band of Fe^{3+} in octahedral coordination like in the $\text{Fe}_2(\text{MoO}_4)_3$ phase [28]. This is also confirmed by the absence of the 460 nm band in the iron-free MC-B (Fig. 4b) catalyst. We may therefore conclude that the iron in our catalysts forms the $\text{Fe}_2(\text{MoO}_4)_3$ phase, which is also supported by the XRD results. The UV-DRS spectra of the Cr-containing catalyst (MC-G) in Fig. 4b shows three maxima at 685, 710 and 745 nm, respectively, with further a broad band at 487 nm, which are characteristic bands of Cr in sixfold oxygen coordination, like in $\text{Cr}_2(\text{MoO}_4)_3$ [32]. The spectra of the Al-containing catalyst (MC-H) did not exhibit any peak that could be specifically ascribed to this metal ion.

Surface Composition of the Catalyst

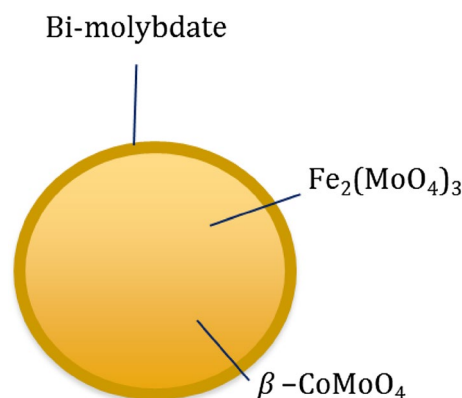
The surface composition of the multicomponent catalyst before and after calcination was determined by X-ray photoelectron spectroscopy (Table 5). The XPS data for

Table 5 Surface composition (atomic percentage) of the MC-A catalyst before and after calcination, as well as after reaction

Elements	Before calcination (%)	After calcination (%)	After reaction (%)
Bi	0.1	1.2	0.21
Co	2.3	0.9	2.2
Ni	2.4	0.7	0.9
Fe	1.3	0.8	1.7
Mo	0.2	8.1	6.7
O	62.4	67.1	65.6
Si	18.3	20.7	22.7

the catalyst MC-A shows the presence of all the elements, i.e., Bi, Mo, Co, Ni, Fe, Si and O at the surface, except P and K, which are not detected most probably due to their very small concentrations. Nevertheless, the results suggest the migration of the bismuth molybdate phase to the surface during calcination of the catalyst. Indeed, the surface of the calcined catalyst is enriched with Bi (1.2 vs 0.1 % before calcination) and Mo (8.1 vs 0.2 % before calcination). Simultaneously, the depletion of Co, Ni and Fe at the surface indicates that these elements migrated towards the inner core of the catalyst during calcination. After the ammoxidation reaction, an enrichment of the surface by Co, Fe and Ni was observed, whereas Bi and Mo slightly depleted, implying the reverse migration of these two elements during the course of reaction. Wolf *et al.* [37] found the presence of only Bi, Mo and O on the surface of $\text{Co}_8\text{Fe}_3\text{BiMo}_{12}\text{O}_x$ and $\text{Mg}_8\text{Fe}_{2.5}\text{BiMo}_{12}\text{O}_x$ catalysts. Based on these results, they suggested a core and shell model structure for the multicomponent catalyst (Fig. 5), where bismuth molybdate is present as a thin layer (about 5–10 nm) on the surface, while the inner core contains a mixture of $\text{Fe}_2\text{Mo}_3\text{O}_{12}$ and $\text{M}^{\text{II}}\text{MoO}_4$ where $\text{M}^{\text{II}} = \text{Co, Ni or Mg}$. However, this model is only partially valid on our catalyst, as we found all the elements on the surface.

Figure 6 shows the XPS spectra of the elements detected on the surface of the calcined MC-A catalyst. One can see that Mo is present as Mo^{6+} with a Mo $3d_{5/2}$ binding energy (BE) of 232.8 eV [38], Bi is present as Bi^{3+} with a Bi $4f_{7/2}$ BE value of 159.9 eV [38], Co is present as Co^{2+} with a Co $2p_{3/2}$ BE value of 781.4 eV [39], Ni as Ni^{2+} with a Ni $2p_{3/2}$ BE value of 855.9 eV [40], Fe is present as Fe^{3+} with a Fe $2p_{3/2}$ BE value of 712.3 eV [41] which is in agreement with the metal molybdate phases observed in XRD. The BE for Si is observed at 104 which is characteristic of Si 2p for SiO_2 [42]. Two distinct types of oxygen were detected, whereby the higher BE one at 533.1 eV was ascribed to O^{I} from the silica binder and the lower BE of O^{II} at 530.8 eV to the different metal oxide species [43]. The ratio of amount of bismuth on the surface to the amount of bivalent

**Fig. 5** Core and shell model of multicomponent catalyst from Wolf *et al.* [37]

M^{II} and trivalent M^{III} metals (where $\text{M}^{\text{II}} = \text{Co, Ni}$ and $\text{M}^{\text{III}} = \text{Fe}$) was calculated for all catalysts of series a) and b), respectively (Fig. 7). The MC-B catalyst without iron showed the highest $\text{Bi}/(\text{M}^{\text{II}} + \text{M}^{\text{III}})$ ratio (0.8) of the evaluated series. Furthermore, the MC-C catalyst containing a Co–Fe–Bi–Mo combination showed a ratio of 0.5 very close to that of the MC-A catalyst (0.52), strongly suggesting a similar composition/arrangement on the surface. On the other hand, the MC-D catalyst containing Ni, and the MC-H catalyst (in which aluminum replaced iron) showed a lower bismuth amount on the surface than the MC-A catalyst (with ratios of 0.1 and 0.3, respectively).

Discussion

Screening of MC Catalysts with Different Bivalent and Trivalent Cations

Among the catalysts screened for acrolein ammoxidation reaction, it can be seen that the bivalent and trivalent metal cations have a remarkable effect on the catalyst performance. For the bivalent metals, the catalyst consisting of both Co and Ni was seen to be more active and selective than when they used alone.

A possible explanation for the superior performance of the Co–Ni-based catalyst (MC-A) catalyst is linked with the existence of the metastable $\beta\text{-Co}_x\text{Ni}_{1-x}\text{MoO}_4$ phase of mixed molybdate of cobalt and nickel. Graselli *et al.* [44] reported that the Ni–Co molybdates show improved activity in propane oxydehydrogenation compared to single metal molybdates, due to their stability. Furthermore, Maione *et al.* [24] studied the solid solutions of Ni and Co molybdates dispersed on silica for propane oxydehydrogenation reaction. They also observed the advantage of the mixed Co–Ni molybdate in comparison with Ni or Co

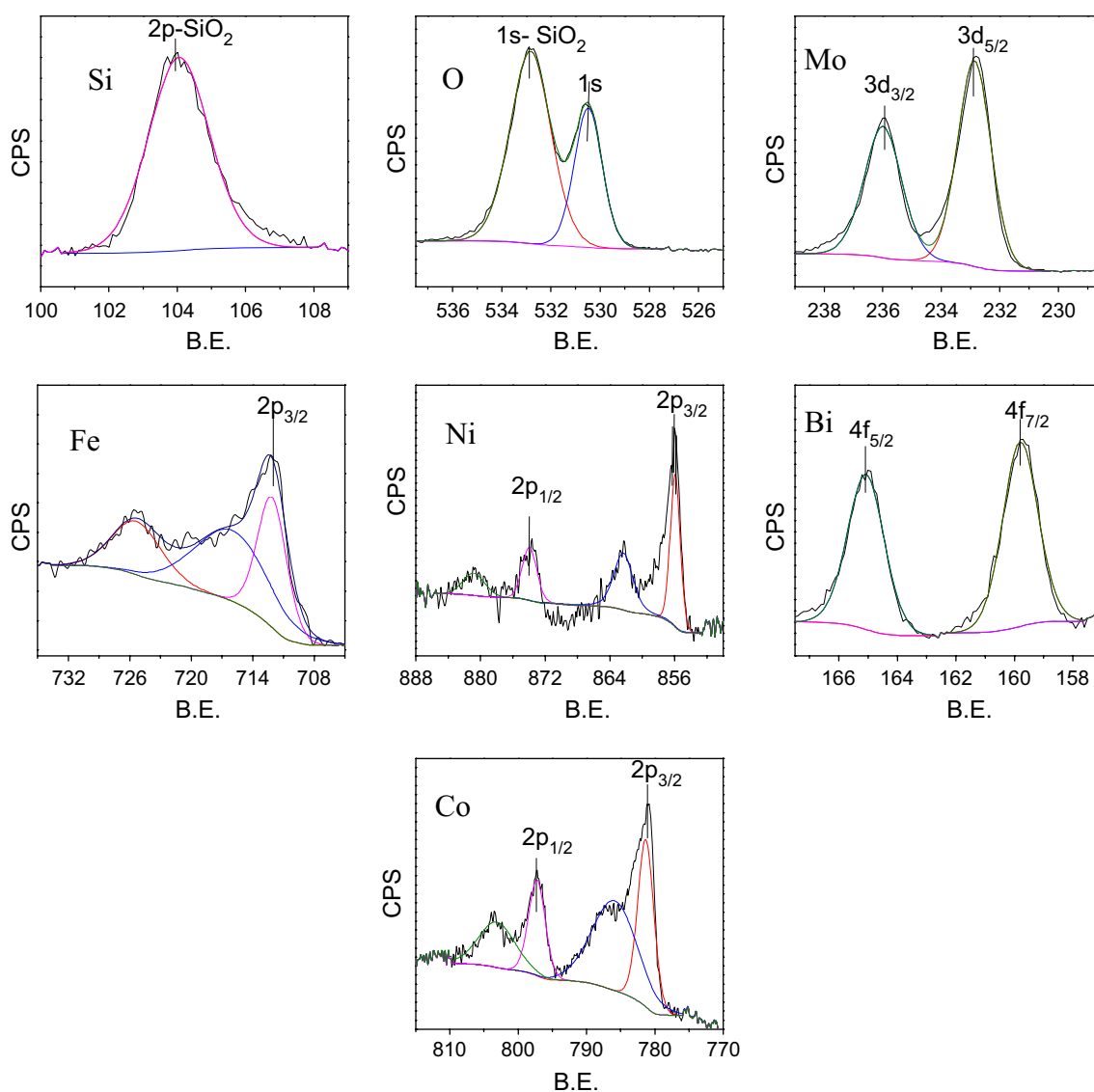


Fig. 6 XPS spectra of MC-A catalyst

molybdates alone, whereas the highest activity was reached over the β - $\text{Co}_x\text{Ni}_{1-x}\text{MoO}_4$ phase. Additionally, the better performances over the MC-A catalyst could be due to a Bi-enriched surface with a $\text{Bi}/(\text{Co} + \text{Ni} + \text{Fe})$ ratio of 0.48 and a larger quantity of γ - Bi_2MoO_6 compared to α - $\text{Bi}_2\text{Mo}_3\text{O}_{12}$ (γ - $\text{Bi}_2\text{MoO}_6/\alpha$ - $\text{Bi}_2\text{Mo}_3\text{O}_{12}$ ratio = 2.6), whereby the former is reported to be more active and selective towards ACN [32, 45]. Concerning the catalysts containing only Co or Ni (MC-C and MC-D, respectively), the higher acrylonitrile yield of the Co-containing catalyst (MC-C) is attributed to the presence of the metastable beta molybdate phase (β - CoMoO_4), whereas the Ni-containing catalyst exhibits the alpha molybdate phase (α - NiMoO_4 in MC-D). It was reported that the presence of tetrahedral coordination of Mo in the β -phase favors the weakly bonded labile surface

complex of acrolein which resulted into partial oxidation, whereas in case of the α -phase (octahedral coordination of Mo), the strongly bonded surface acrolein complexes leads to the total oxidation forming CO_x [46]. Moreover, high selectivity to ACN of the Co (MC-C) catalyst could also be attributed to the large γ - $\text{Bi}_2\text{MoO}_6/\alpha$ - $\text{Bi}_2\text{Mo}_3\text{O}_{12}$ ratio of 4.37 calculated from XRD peaks relative heights, which implies, as least in the bulk, a larger quantity of γ - Bi_2MoO_6 compared to that of α - $\text{Bi}_2\text{Mo}_3\text{O}_{12}$. Furthermore, the Co-based catalyst also exhibits a surface enriched in Bi with a $\text{Bi}/(\text{Co} + \text{Ni} + \text{Fe})$ ratio of 0.52, which is slightly higher than the ratio in the MC-A catalyst (0.48).

The MC-F catalyst containing Mg as a bivalent element shows an acrolein conversion of 79 % with a selectivity to acrylonitrile of 46 %, giving an overall yield of 37 %,

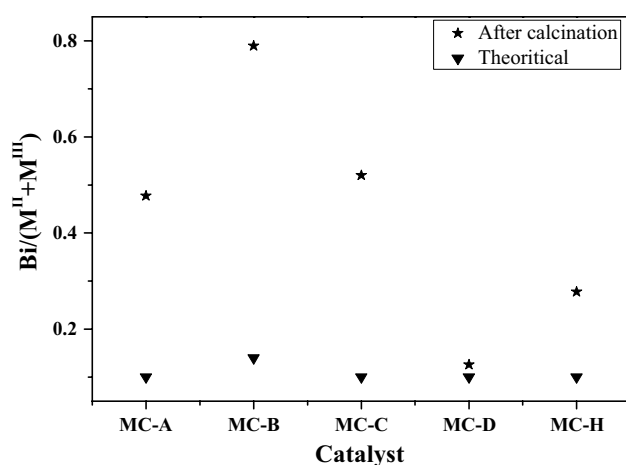


Fig. 7 Surface ($\text{Bi}/\text{M}^{\text{II}} + \text{M}^{\text{III}}$) ratio of the multicomponent catalysts calculated from XPS

which is similar to that of the Ni-containing catalyst (MC-D). The lower activity of Mg molybdate, compared to Co and Ni molybdates was already observed by Wolf *et al.* [32] for the selective oxidation of *I*-butene. Haber *et al.* [47] reported that the lower activity of Mg^{2+} complexes is due to their very weak bonding with allylic species in the propylene oxidation compared to Co^{2+} and Ni^{2+} species.

It was observed that the presence of trivalent cation (especially Fe) in the MC catalyst has positive effect on its catalytic performance. The effect of iron can be explained from the molybdate phase formation as observed by XRD. In the catalyst prepared without iron (MC-B), the $\alpha\text{-Bi}_2\text{Mo}_3\text{O}_{12}$ phase (relative intensity 71.2) is formed predominantly compared to the gamma phase ($\gamma\text{-Bi}_2\text{MoO}_6$; relative intensity 43.7) with a $\gamma\text{-Bi}_2\text{MoO}_6/\alpha\text{-Bi}_2\text{Mo}_3\text{O}_{12}$ ratio of 0.6. However, the catalyst with iron (MC-A) has $\gamma\text{-Bi}_2\text{MoO}_6$ as a dominant phase with a ratio of 2.6. This implies that iron promotes the formation of the $\gamma\text{-Bi}_2\text{MoO}_6$ phase rather than that of the $\alpha\text{-Bi}_2\text{Mo}_3\text{O}_{12}$ phase, as already reported by Batist *et al.* [28] for the addition of Fe_2O_3 and Cr_2O_3 . A similar observation was also reported by Wolf *et al.* [32] who claimed that the relative intensity ratio of $\gamma\text{-Bi}_2\text{MoO}_6/\alpha\text{-Bi}_2\text{Mo}_3\text{O}_{12}$ increases with increasing the iron content of the catalyst, confirming the promotion effect of iron on the $\gamma\text{-Bi}_2\text{MoO}_6$ phase formation. The XRD study showed that the Co–Ni–Fe–Bi catalyst (MC-A) exhibited the exclusive formation of the metastable $\beta\text{-Co}_x\text{Ni}_{1-x}\text{MoO}_4$ phase for Co–Ni molybdate while the iron-free Co–Ni–Bi catalyst showed the formation of the $\alpha\text{-Co}_x\text{Ni}_{1-x}\text{MoO}_4$ phase along with the β -type phase. This indicates that the metastable $\beta\text{-Co}_x\text{Ni}_{1-x}\text{MoO}_4$ phase is stabilized in the presence of iron. Wolf *et al.* [32] drew up the explanation that in the α -phase, both metal ion and Mo are in octahedral oxygen coordination and connected via the edges. However, in the β -phase, the metal ions are in octahedral

coordination and Mo is in tetrahedral coordination and connection occurs via the corners, as in the case of the $\text{Fe}_2(\text{MoO}_4)_3$ phase (Fe–O octahedra and Mo–O tetrahedra). Furthermore, the sequence of layers of Co, Mo and of Fe, Mo along the *c*-axes is closely similar. Therefore, the predominance of the β -phase instead of the α -phase in the presence of iron can be explained by assuming that the β -phase structure is better suited to fit the $\text{Fe}_2(\text{MoO}_4)_3$ lattice structure.

Trivalent cations, and especially iron, are also reported to have several roles in the multicomponent catalysts. Grasselli [13] stated that iron serves as an efficient redox couple ($\text{Fe}^{3+/2+}$), capable of efficient lattice oxygen transfer to the Bi–Mo–O active site in its Fe^{3+} oxidation state. Indeed, in its 2+ oxidation state, it efficiently chemisorbs dioxygen and dissociates it to lattice oxygen (O^{2-}) with further incorporation into the lattice. Since during the reaction it is difficult to maintain a sufficient number of Fe^{2+} surface sites in an overall oxidizing gaseous atmosphere, it is necessary to structurally stabilize the Fe^{2+} state. In this scenario, divalent elements like Co, Ni and Mg form stable molybdates isostructural to Fe^{2+} molybdate, and thus stabilize the Fe^{2+} state. In other words, Ni, Co and Mg have the function of providing the host structure for Fe^{2+} in the multiphase catalysts.

Parameter Optimization

After the fundamental study described above, we wanted to find the best reaction conditions for obtaining a high yield in acrylonitrile. Therefore, inspired by the promising results of the MC-A catalyst, an experimental design was carried out in order to optimize the key reaction parameters: reaction temperature, NH_3/AC and contact time.

The model in Fig. 8 represents the effect of the variation of reaction temperature and NH_3/AC ratio on the conversion of acrolein. The acrolein conversion increased with both the reaction temperature and the NH_3/AC ratio. The minimum of conversion was predicted for 350 °C and at a NH_3/AC ratio of 1 (64 %). It then gradually increased with the temperature, whereby a maximum of 90 % was predicted at 425 °C with a NH_3/AC ratio of around 2. This is most probably linked to the fact that a high temperature is required for the activation of ammonia.

Figure 9 shows the influence of the reaction temperature and of the NH_3/AC molar ratio on the acrylonitrile yield. The lowest yield was predicted at 350 °C (18 %), irrespective of the NH_3/AC ratio. This yield increased with the reaction temperature, and the highest yield was predicted at 425 °C. Concerning the NH_3/AC ratio, the highest yield of 61 % was predicted for a NH_3/AC ratio of around 2.

The influence of contact time and of the NH_3/AC molar ratio on the acrylonitrile yield at constant temperature

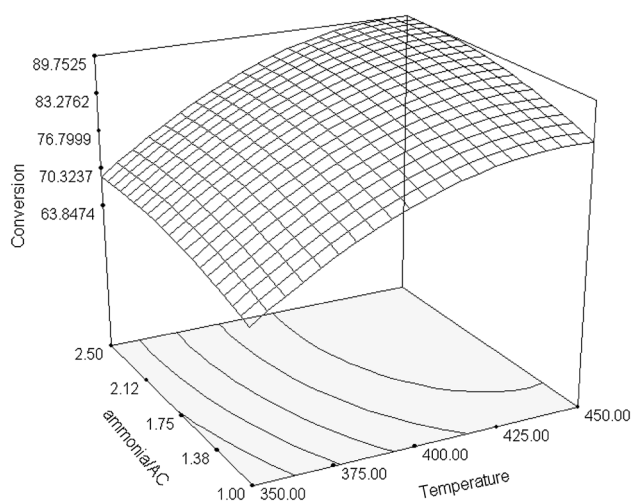


Fig. 8 Acrolein (AC) conversion as a function of the reaction temperature and the NH_3/AC molar ratio at constant contact time. Reaction conditions: pressure—1 bar, contact time—0.5 s, acrolein/ O_2 ratio—0.38

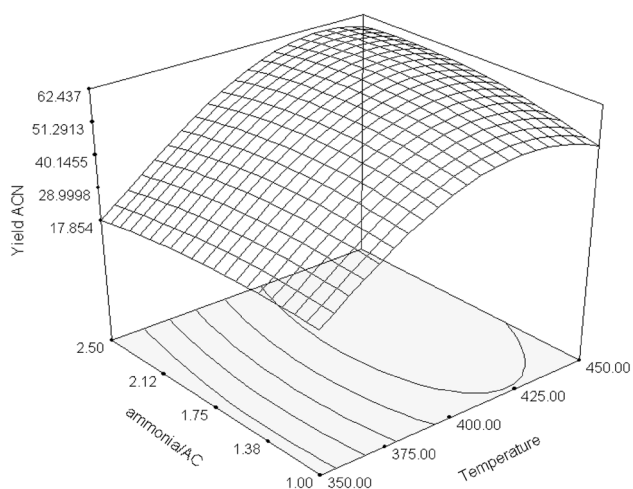


Fig. 9 Acrylonitrile (ACN) yield as a function of the reaction temperature and the NH_3/AC molar ratio at constant contact time. Reaction conditions: pressure—1 bar, contact time—0.5 s, acrolein/ O_2 ratio—0.38

(400 °C) is depicted in Fig. 10. The lowest acrylonitrile yield of 47 % was predicted at the higher contact time of 1.5 s and an NH_3/AC ratio of 1. For low NH_3/AC ratios, an increase in the yield is predicted with decreasing contact time, whereby the highest yield was predicted for a contact time of 0.5 s. Furthermore, the acrylonitrile yield was predicted to show an optimum with respect to the NH_3/AC ratio whereby the highest yield was predicted for a ratio of 2.

In order to validate the model, the parameters predicting the highest catalytic performance (temperature of 425 °C,

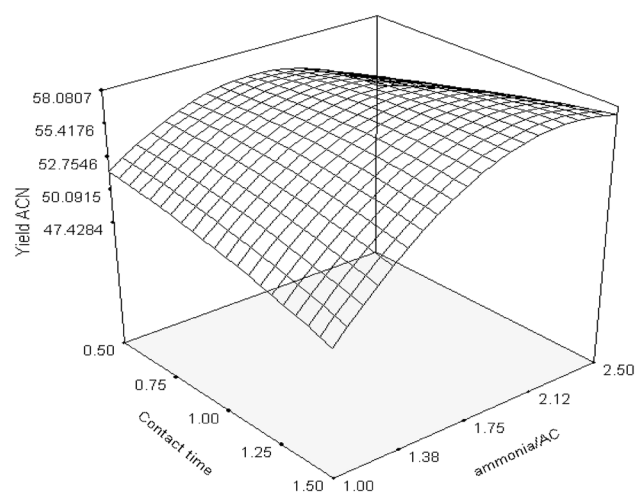


Fig. 10 Acrylonitrile (ACN) yield as a function of the contact time and the NH_3/AC molar ratio at constant reaction temperature. Reaction conditions: pressure—1 bar, reaction temperature—400 °C, acrolein/ O_2 ratio—0.38

Table 6 Comparison of predicted and real results for optimized parameters

Catalyst	Experiment	Conversion AC (%)	Selectivity ACN (%)	Yield ACN (%)
MC-A	Predicted	90	67	62
MC-A	Measured	93	63	59

Reaction conditions: pressure—1 bar, reaction temperature—425 °C, contact time—0.5 s, NH_3/AC ratio—2

NH_3/AC molar ratio of 2 and contact time of 0.5 s) were experimentally verified. From the results (Table 6), one can see that the experimental and predicted values were very close, as the observed acrolein conversion was of 93 *versus* 90 % for the value predicted by the model issued from DOE. The observed selectivity to acrylonitrile was 63 *versus* 67 % for the prediction, and, therefore, the obtained overall yield of acrylonitrile was 59 *versus* 62 % for the predicted value, which confirms the excellent agreement between the experimental values and the model-derived values, thus validating the model. It is further worth mentioning that the catalyst performance remained stable for 10 h as shown in Fig. 11.

Comparing the literature values for acrylonitrile yield, there are only two catalytic systems which were reported as giving a higher acrylonitrile yield than the MC-A catalyst in this study (59 %), namely a tin antimony oxide catalyst (74 %) [48] and an As–Fe–O mixed oxide catalysts (87 %) [11]. However, the results reported with tin antimony oxide catalyst were in absence of water in the reaction feed, and the high toxicity of arsenic makes the application of the latter catalyst difficult in an industrial process.

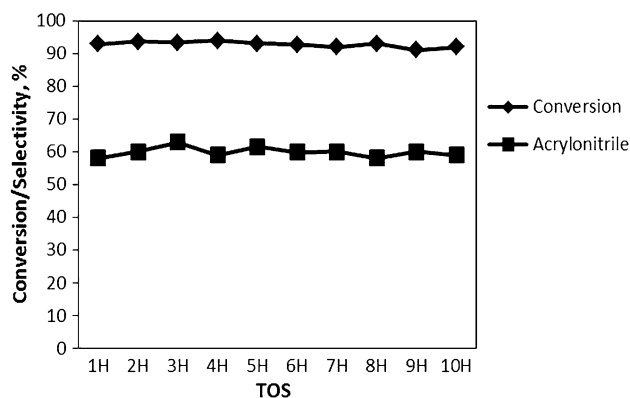


Fig. 11 Catalytic performance of MC-A plotted over time on stream. Reaction conditions: pressure—1 bar, reaction temperature—425 °C, contact time—0.5 s, NH_3/AC ratio—2

Conclusion

The multicomponent Bi-Mo catalysts are very active and selective in the reaction of acrolein ammoxidation to acrylonitrile. The activity of the multicomponent catalyst is significantly affected by the choice of the bivalent and trivalent metal cations. Among bivalent cations, the catalysts containing a mixture of Co and Ni showed the highest activity and selectivity. In fact, the formation of a metastable β -phase of $\text{M}^{\text{II}}\text{MoO}_4$ and Bi-enriched surface was responsible for the higher performance of Co–Ni- and Co-containing catalysts, whereas the lower activity of the only Ni-containing catalyst was due to the presence of the α - NiMoO_4 phase.

The role of the trivalent element is crucial because it is supposed to provide an efficient redox cycle in the ammoxidation reaction. We also observed that there is a significant decrease in the catalytic performances in the absence of iron. The characterization study showed that iron has a significant promoting effect on the formation of the metastable β -phase of $\text{M}^{\text{II}}\text{MoO}_4$ and of the Koehlinite γ - Bi_2MoO_6 phase of bismuth, which leads to a better activity of the iron-containing catalysts. Among the trivalent metal-containing catalysts, the activity order was observed as $\text{Fe} > \text{Al} > \text{Cr}$ in terms of acrylonitrile yield.

Finally, the highest performance of 59 % yield in ACN was found for the MC-1 reference catalyst at 425 °C with a NH_3/AC molar ratio of 2 and a contact time of 0.5 s.

Acknowledgments The *Fonds Européen de Développement Régional* (FEDER), *CNRS, Région Nord Pas-de-Calais* and *Ministère de l'Éducation Nationale de l'Enseignement Supérieur et de la Recherche* are acknowledged for fundings of XPS/LEIS/ToF-SIMS spectrometers within the Pôle Régional d'Analyses de Surface. Chevreul Institute (FR 2638), Ministère de l'Enseignement Supérieur et de la Recherche, Région Nord – Pas de Calais and FEDER are acknowledged for supporting and funding partially this work.

References

- <https://www.agra-net.net/agra/world-ethanol-and-biofuels-report/biofuel-news/biodiesel/european-union-council-approves-7-cap-for-crop-based-biofuels-442927.htm>
- OECD-FAO Agricultural Outlook 2011–2020. <http://www.agri-outlook.org>
- Katryniok B, Paul S, Dumeignil F (2013) Recent developments in the field of catalytic dehydration of glycerol to acrolein. *ACS Catal* 3(8):1819–1834
- Guerrero-Perez MO, Banares MA (2008) New reaction: conversion of glycerol into acrylonitrile. *ChemSusChem* 1(6):511–513
- Liebig C, Paul S, Katryniok B, Guillon C, Couturier J-L, Dubois J-L, Dumeignil F, Hoelderich WF (2013) Glycerol conversion to acrylonitrile by consecutive dehydration over WO_3/TiO_2 and ammoxidation over $\text{Sb}(\text{Fe}, \text{V})\text{-O}$. *Appl Catal B* 132–133:170–182
- Bradzil JF (2000) Acrylonitrile. *Kirk-Othmer encyclopedia of chemical technology*. Wiley, New York. doi:10.1002/0471238961.0103182502180126.a01.pub3
- Knox W, Taylor K, Tullman G (1974) Ammoxidation of saturated hydrocarbons. US-patent US3833638A
- Dubois J-L (2008) Method for the synthesis of acrylonitrile from glycerol. US-patent US20100048850A1
- Liebig C, Paul S, Katryniok B, Guillon C, Couturier J-L, Dubois J-L, Dumeignil F, Hoelderich WF (2014) Reply to the Letter to the Editor concerning the comments of M.A. Banares and M.O. Guerrero-Pérez to the article “Glycerol conversion to acrylonitrile by consecutive dehydration over WO_3/TiO_2 and ammoxidation over $\text{Sb}(\text{Fe}, \text{V})\text{-O}$ ”. *Appl Catal B* 148–149:604–605
- Bañares MA, Guerrero-Pérez MO (2014) Comments on “Glycerol conversion to acrylonitrile by consecutive dehydration over WO_3/TiO_2 and ammoxidation over $\text{Sb}(\text{Fe}, \text{V})\text{-O}$ ”. *Appl Catal B* 148–149:601–603
- Vanderborgh H (1963) Procédé de préparation de nitriles non saturés. Belgium Patent BE 628287
- Oka H, Miyake K, Harano Y, Imoto T (1975) *J Appl Chem Biotechnol* 25:663–670
- Grasselli RK (1999) Advances and future trends in selective oxidation and ammoxidation catalysis. *Catal Today* 49(1–3):141–153
- Kung HH, Kung MC (1985) Selective oxidative dehydrogenation of butenes on ferrite catalysts. *Adv Catal* 33:159–198
- Moro-Oka Y, Ueda W (1994) Multicomponent bismuth molybdate catalyst: a highly functionalized catalyst system for the selective oxidation of olefin. *Adv Catal* 40:233–273
- Gunter S, Joachim K, Kurt S, Rolf S, Wilhelm V (1965) Process for preparing unsaturated nitriles. US-patent US3226422
- Takenaka S, Yamaguchi G (1969) Process for the oxidation of olefins to aldehydes and acids. US-patent US3454630A
- Idol JJ (1973) Process for the manufacture of acrylonitrile and methacrylonitrile. US-patent US2904580 A
- Kolchin I, Galperin E, Bobkov S, Margolis LY (1964) Oxidation of propylene on a bismuth-molybdenum catalyst. *Neftekhimiya* 4:301
- German K, Grzybowka B, Haber J (1973) Active centers for oxidation of propylene on Bi-Mo-O catalysts. *Bull Acad Pol Sci Ser Sci Chim* 21:319
- Monnier JR, Keulks GW (1979) *Am Chem Soc Div Pet Chem* 24:19
- Burrington JD, Grasselli RK (1979) Aspects of selective oxidation and ammoxidation mechanisms over bismuth molybdate catalysts. *J Catal* 59(1):79–99
- Carson D, Coudurier G, Forissier M, Vedrine JC, Laarif A, Theobald F (1983) Synergy effects in the catalytic properties of

- bismuth molybdates. *J Chem Soc Faraday Trans 1 Phys Chem Condens Phases* 79(8):1921–1929
24. Maione A, Devillers M (2004) Solid solutions of Ni and Co molybdates in silica-dispersed and bulk catalysts prepared by sol–gel and citrate methods. *J Solid State Chem* 177(7):2339–2349
 25. Ono T, Ogata N, Miyaryo Y (1996) Characteristic features of Raman band shifts of scheelite-type molybdate catalysts exchanged with the ^{18}O tracer via redox reactions. *J Catal* 161(1):78–86
 26. Maldonado-Hódar FJ, Palma Madeira LM, Farinha Portela M (1996) The effects of coke deposition on NiMoO_4 used in the oxidative dehydrogenation of butane. *J Catal* 164(2):399–410
 27. Mazzocchia C, Aboumradi C, Diagne C, Tempesti E, Herrmann J, Thomas G (1991) On the NiMoO_4 oxidative dehydrogenation of propane to propene: some physical correlations with the catalytic activity. *Catal Lett* 10(3–4):181–191
 28. Batist PA, van de Moesdijk CGM, Matsuura I, Schuit GCA (1971) The catalytic oxidation of 1-butene over bismuth molybdates: promoters for the $\text{Bi}_2\text{O}_3\cdot 3\text{MoO}_3$ catalyst. *J Catal* 20(1):40–57
 29. Harrison WTA (1995) Crystal structures of paraelastic aluminum molybdate and ferric molybdate, $\beta\text{-Al}_2(\text{MoO}_4)_3$ and $\beta\text{-Fe}_2(\text{MoO}_4)_3$. *Mater Res Bull* 30(11):1325–1331
 30. Battle PD, Cheetham AK, Harrison WTA, Pollard NJ, Faber J Jr (1985) The structure and magnetic properties of chromium(III) molybdate. *J Solid State Chem* 58(2):221–225
 31. Carrazan S, Martin C, Rives V, Vidal R (1996) An FT-IR spectroscopy study of the adsorption and oxidation of propene on multiphase Bi, Mo and Co catalysts. *Spectrochim Acta Part A Mol Biomol Spectrosc* 52(9):1107–1118
 32. Wolfs MWJ, Batist PHA (1974) The selective oxidation of 1-butene over a multicomponent molybdate catalyst. Influences of various elements on structure and activity. *J Catal* 32(1):25–36
 33. Giordano N, Padovan M, Vaghi A, Bart JCI, Castellan A (1975) Structure and catalytic activity of $\text{MoO}_3\cdot\text{Al}_2\text{O}_3$ systems: III. Nature of sites for propylene disproportionation. *J Catal* 38(1–3):1–10
 34. Smith G, Ibers J (1965) The crystal structure of cobalt molybdate CoMoO_4 . *Acta Crystallogr A* 19(2):269–275
 35. Zhou C-J, Huang C-J, Zhang W-G, Zhai H-S, Wu H-L, Chao Z-S (2007) Synthesis of micro- and mesoporous ZSM-5 composites and their catalytic application in glycerol dehydration to acrolein. *Stud Surf Sci Catal* 165:527–530
 36. Zhang YJ, Rodríguez-Ramos I, Guerrero-Ruiz A (2000) Oxidative dehydrogenation of isobutane over magnesium molybdate catalysts. *Catal Today* 61(1–4):377–382
 37. Matsuura I, Wolfs MWJ (1975) X-ray photoelectron spectroscopy study of some bismuth molybdates and multicomponent molybdates. *J Catal* 37(1):174–178
 38. Uchida K, Ayame A (1996) Dynamic XPS measurements on bismuth molybdate surfaces. *Surf Sci* 357–358:170–175
 39. Armour AW, Mitchell PCH, Folkesson B, Larsson R (1974) X-ray photoelectron (ESCA) spectra of some molybdenum-containing catalysts. *J Less Common Metals* 36(1–2):361–365
 40. Kaddouri A, Tempesti E, Mazzocchia C (2004) Comparative study of β -nickel molybdate phase obtained by conventional precipitation and the sol–gel method. *Mater Res Bull* 39(4–5):695–706
 41. Soares APV, Portela MF, Kiennemann A, Hilaire L (2003) Mechanism of deactivation of iron-molybdate catalysts prepared by coprecipitation and sol–gel techniques in methanol to formaldehyde oxidation. *Chem Eng Sci* 58(7):1315–1322
 42. Coulter KE, Sault AG (1995) Effects of activation on the surface properties of silica-supported cobalt catalysts. *J Catal* 154(1):56–64
 43. Rao TSRP, Menon PG (1978) Physicochemical studies on silica-supported multicomponent molybdate catalyst before and after use in ammoxidation of propylene. *J Catal* 51(1):64–71
 44. Grasselli RK, Burrington JD (1981) Selective oxidation and ammoxidation of propylene by heterogeneous catalysis. *Adv Catal* 30:133–163
 45. Jung JC, Lee H, Kim H, Chung Y-M, Kim TJ, Lee SJ, Oh S-H, Kim YS, Song IK (2008) Effect of oxygen capacity and oxygen mobility of pure bismuth molybdate and multicomponent bismuth molybdate on their catalytic performance in the oxidative dehydrogenation of n-butene to 1, 3-butadiene. *Catal Lett* 124(3–4):262–267
 46. Zakharov II, Popova GY, Andrushkevich TV (1982) Effect of molybdenum ion coordination on acrolein adsorption on α - and β -cobalt molybdate. *React Kinet Catal Lett* 19(3–4):367–371
 47. Haber J, Witko M (1981) Quantum-chemistry and catalysis in oxidation of hydrocarbons. *Acc Chem Res* 14(1):1–7
 48. Wood B (1962) Production of unsaturated aliphatic nitriles. US-patent US3094552 A